

## Dangling Carboxylic Group That Participates in O–O Bond Formation Reaction to Promote Water Oxidation Catalyzed by a Ruthenium Complex: Experimental Evidence of an Oxide Relay Pathway

Animesh Kundu, Suman K. Barman, and Sukanta Mandal\*

Cite This: *Inorg. Chem.* 2022, 61, 1426–1437

Read Online

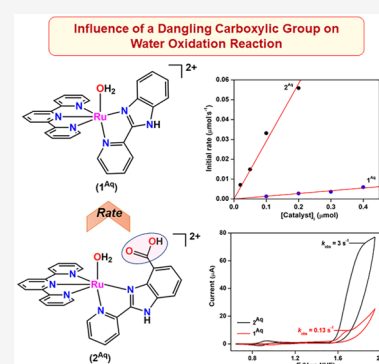
ACCESS |

Metrics & More

Article Recommendations

Supporting Information

**ABSTRACT:** Two mononuclear ruthenium(II) complexes of the types  $[\text{Ru}(\text{trpy})(\text{HL}^1)(\text{OH}_2)]^{2+}$  ( $1^{\text{Aq}}$ ) and  $[\text{Ru}(\text{trpy})(\text{L}^2\text{-}\kappa\text{-N}^2\text{O})]$  ( $2$ ) [where  $\text{trpy} = 2,2':6',2''$ -terpyridine,  $\text{HL}^1 = 2$ -(2-pyridyl)benzimidazole,  $\text{H}_2\text{L}^2 = 2$ -(pyridin-2-yl)-1*H*-benzo[*d*]imidazole-4-carboxylic acid] have been synthesized and thoroughly characterized by analytical and spectroscopic [UV–vis, NMR, high-resolution mass spectrometry, and IR] techniques. Complex  $1^{\text{Aq}}$  has been further characterized by X-ray crystallography. In an acidic aqueous medium (pH 1), complex  $2$  undergoes carboxylate/water exchange readily to form an aqua-ligated complex,  $[\text{Ru}(\text{trpy})(\text{H}_2\text{L}^2\text{-}\kappa\text{-N}^2)(\text{OH}_2)]^{2+}$  ( $2^{\text{Aq}}$ ), having a dangling carboxylic group. This exchange phenomenon has been followed by IR,  $^1\text{H}$  NMR, and UV–vis spectroscopic techniques. Electrochemical analyses of  $1^{\text{Aq}}$  and  $2^{\text{Aq}}$  (Pourbaix diagram) suggest the generation of a formal  $\text{Ru}^{\text{V}}=\text{O}$  species that can potentially promote the oxidation of water. A comparative study of the water oxidation activity catalyzed by  $1^{\text{Aq}}$  and  $2^{\text{Aq}}$  is reported here to see the effect of a dangling carboxylic group in the catalytic performance. Complex  $2^{\text{Aq}}$  shows an enormously higher rate of reaction than  $1^{\text{Aq}}$ . The pendant carboxylic group in  $2^{\text{Aq}}$  participates in an intramolecular O–O bond formation reaction with the reactive formal  $\text{Ru}^{\text{V}}=\text{O}$  unit to form a percarboxylate intermediate and provides an electron-deficient carbon center where water nucleophilic attack takes place. The isotope labeling experiment using  $^{18}\text{O}$ -labeled water verifies the attack of water at the carbon center of the carboxylic group rather than a direct attack at the oxo of the formal  $\text{Ru}^{\text{V}}=\text{O}$  unit. The present work provides experimental evidence of the uncommon functionality of the carboxylic group, the oxide relay, in molecular water oxidation chemistry.



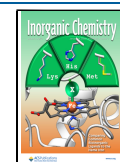
### INTRODUCTION

The generation of hydrogen fuel by splitting of water is a promising strategy to develop an environmentally friendly and sustainable energy economy.<sup>1–4</sup> In this endeavor, the water oxidation step is the major concern because it is an energetically challenging reaction with enormous complexity. During water oxidation reaction, removal of hydrogen atoms ( $\text{H}^+ + \text{e}^-$ ) from a water molecule and the making of an O–O bond are two major aspects that a catalyst should execute effectively.<sup>5–8</sup> To develop an effective catalyst, the judicious design of a ligand is essential. In recent years, strategies are taken to design ligands that not only govern the primary coordination sphere but also fine-tune the secondary interactions.<sup>9–15</sup> In this regard, the design of molecular catalysts containing a carboxylate functional group in the ligand scaffold has gained much attention in order to develop efficient water oxidation catalysts (WOCs), particularly with ruthenium metal ions.<sup>11–13,16–18</sup> In a natural oxygen-evolving complex of photosystem II, the manganese ions are surrounded by numerous negatively charged oxo and carboxylate ligands that provide a coordination environment

as well as modulate the reactivity by forming a hydrogen bond with incoming water.<sup>19</sup> The carboxylate moiety in a ligand can play diverse roles to control the catalytic performances of metal complexes. It can actively stabilize the high-valent states of metal complexes owing to its strong  $\sigma$ -donating ability. In Sun's  $\text{Ru}(\text{bda})$  complex, the strong  $\sigma$  donation from the two carboxylate groups has allowed one to access the reactive  $[\text{Ru}^{\text{V}}(\text{O})(\text{bda})(\text{pic})_2]^+$  species ( $\text{H}_2\text{bda} = 2,2'$ -bipyridine-6,6'-dicarboxylic acid;  $\text{pic} = 4$ -picoline) at a much lower overpotential.<sup>12</sup> In Llobet's  $\text{Ru}(\text{tda})$  molecular catalyst ( $\text{H}_2\text{tda} = [2,2':6',2''\text{-terpyridine}]-6,6''\text{-dicarboxylic acid}$ ), the dangling carboxylate group acts as a pendant base that assists proton-coupled electron-transfer (PCET) processes through intramolecular proton relay and also plays a significant role in

Received: October 6, 2021

Published: January 4, 2022

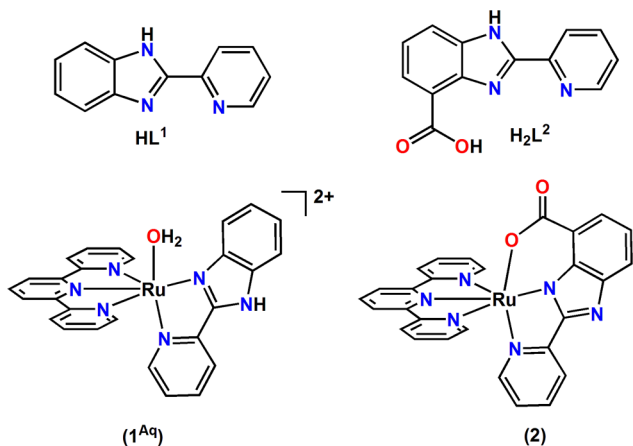


reducing the energy barrier of the rate-limiting O–O bond formation step through its hydrogen-bonding interactions, allowing one to achieve a very high turnover frequency.<sup>13</sup> It has been found that the carboxylate<sup>13</sup> or phosphonate<sup>14</sup> groups present in the secondary coordination sphere of ruthenium-based WOCs work well as proton acceptors at neutral-to-basic pH conditions, while the anionic sulfonate group can facilitate proton relay even in strong acidic conditions during catalysis.<sup>15</sup>

Beside those various functionalities, Ahlquist et al. revealed one more unique function of the carboxylate—the oxide relay—by density functional theory (DFT) calculations.<sup>20</sup> The calculations with  $[\text{Ru}(\text{tda})(\text{py})_2]$  ( $\text{py}$  = pyridine) show that, instead of water nucleophilic attack (WNA) directly at  $\text{Ru}^{\text{V}}=\text{O}$ , the closely placed pendant carboxylate promptly reacts with oxo to form a O–O bond and facilitates water oxidation via an oxide relay pathway. This oxide relay functionality of the pendant carboxylate group is anticipated to be the key reason to achieve an extremely high reaction rate with the  $[\text{Ru}(\text{tda})(\text{py})_2]$  complex.<sup>20</sup> However, experimental evidence for the oxide relay pathway are yet to be achieved to validate the proposal.

Motivated by this diverse functionality of the carboxylic group, we intend to investigate the effect of the carboxylic moiety on the catalytic performance in a comparative manner. For this purpose, we have chosen a reported mononuclear complex,  $[\text{Ru}(\text{trpy})(\text{HL}^1)(\text{OH}_2)]^{2+}$  ( $\mathbf{1}^{\text{Aq}}$ ),<sup>21</sup> and developed a new mononuclear complex,  $[\text{Ru}(\text{trpy})(\text{L}^2-\kappa\text{-N}^2\text{O})]$  ( $\mathbf{2}$ ), where  $\text{trpy}$  = 2,2':6',2''-terpyridine,  $\text{HL}^1$  = 2-(2-pyridyl)-benzimidazole, and  $\text{H}_2\text{L}^2$  = 2-(pyridin-2-yl)-1*H*-benzo[*d*]-imidazole-4-carboxylic acid (Chart 1). In an acidic medium,

Chart 1. Ruthenium(II) Complexes Studied in This Work



exchange of carboxylate/water occurs in complex  $\mathbf{2}$  to generate a catalytically important aqua-ligated complex,  $[\text{Ru}(\text{trpy})(\text{H}_2\text{L}^2-\kappa\text{-N}^2)(\text{OH}_2)]^{2+}$  ( $\mathbf{2}^{\text{Aq}}$ ), having a dangling carboxylic acid group. Herein, we report a comparative water oxidation activity catalyzed by complexes  $\mathbf{1}^{\text{Aq}}$  and  $\mathbf{2}^{\text{Aq}}$  in an acidic medium (pH 1). Complex  $\mathbf{2}^{\text{Aq}}$  shows a higher catalytic performance than  $\mathbf{1}^{\text{Aq}}$ . The presence of a dangling carboxylic group in complex  $\mathbf{2}^{\text{Aq}}$  enhances the reaction rate several times. By performing an isotope experiment, using  $^{18}\text{O}$ -labeled water under catalytic condition, we found evidence of the incorporation of a heavier oxygen isotope into the carboxylic group, validating the oxide relay mechanism. Thus, the present work provides new mechanistic insight toward water oxidation through the

participation of a pendant carboxylic group in the O–O bond formation reaction.

## RESULTS AND DISCUSSION

**Synthesis and Characterizations.** The compound  $[\text{Ru}(\text{trpy})(\text{HL}^1)(\text{OH}_2)](\text{ClO}_4)_2 \cdot \text{H}_2\text{O}$  [ $\mathbf{1}^{\text{Aq}}(\text{ClO}_4)_2 \cdot \text{H}_2\text{O}$ ] was synthesized from its chloro precursor  $[\text{Ru}(\text{trpy})(\text{HL}^1)(\text{Cl})](\text{ClO}_4) \cdot \text{CH}_3\text{CN} \cdot \text{H}_2\text{O}$  [ $\mathbf{1}^{\text{Cl}}(\text{ClO}_4) \cdot \text{CH}_3\text{CN} \cdot \text{H}_2\text{O}$ ] by treatment with  $\text{AgNO}_3$  in water under refluxing conditions, following the literature procedure.<sup>21</sup> The neutral nitrogen of the benzimidazole group coordinates with the ruthenium(II) center. The chloro- and aqua-ligated complexes were characterized by elemental analysis and by various spectroscopic techniques (see the Experimental Section and Figures S1–S9). The molecular structure of  $\mathbf{1}^{\text{Aq}}$  has been determined by single-crystal X-ray crystallography (Figure 1 and Tables S1 and S2).

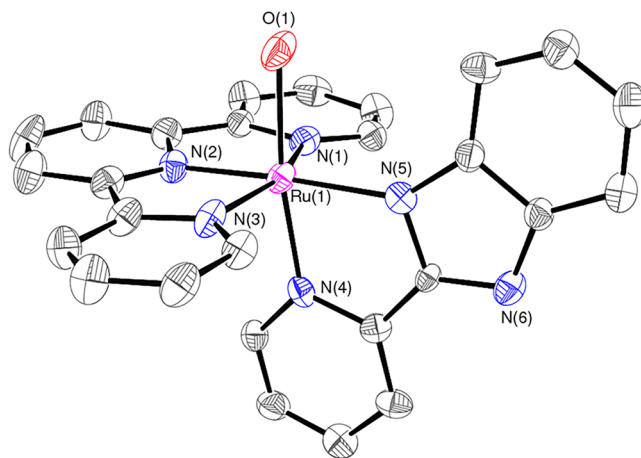
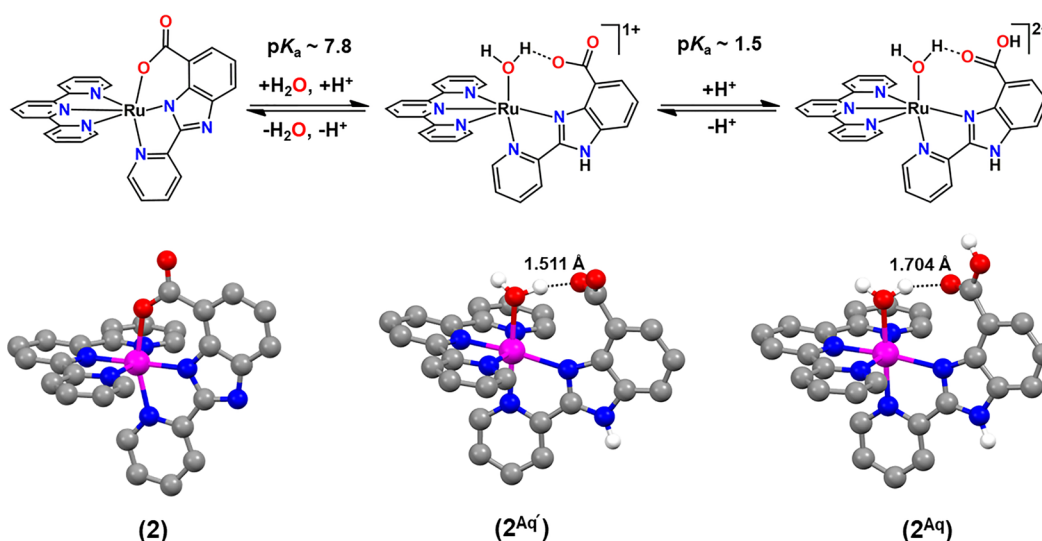


Figure 1. ORTEP (20%) view of the metal coordination environment in the crystal of  $\mathbf{1}^{\text{Aq}}(\text{ClO}_4)_2 \cdot \text{H}_2\text{O}$ . Carbon atoms are not labeled. Hydrogen atoms are omitted for clarity.

The complex has a distorted octahedral geometry where terpyridine coordinates in a meridional fashion and the ligand  $\text{HL}^1$  coordinates in a cis orientation. The sixth coordination site is occupied by an aqua molecule. The pyridyl nitrogen of the  $\text{HL}^1$  ligand and the aqua group are in trans position, confirming isolation of the isomer, as depicted in Chart 1.

The ligand  $\text{H}_2\text{L}^2$  was synthesized via a different route from that reported earlier.<sup>22</sup> In a one-pot reaction, 1:1 condensation of 2-amino-3-nitrobenzoic acid with 2-pyridinecarboxaldehyde produced the Schiff base product, which upon four-electron reduction by  $\text{Na}_2\text{S}_2\text{O}_4$  resulted in the ligand 2-(pyridin-2-yl)-1*H*-benzo[*d*]imidazole-4-carboxylic acid ( $\text{H}_2\text{L}^2$ ). The ligand was characterized by NMR ( $^1\text{H}$  and  $^{13}\text{C}$ ) spectroscopy (Figures S10 and S11). A strong band at  $1700\text{ cm}^{-1}$  was observed in the IR spectrum due to the  $\nu(\text{C}=\text{O})_{\text{asym}}$  stretching vibration of the  $-\text{COOH}$  group (Figure S12). The reaction of  $\text{H}_2\text{L}^2$  with  $[\text{Ru}(\text{trpy})\text{Cl}_3]$  in methanol in the presence of excess triethylamine under refluxing conditions and an inert atmosphere yielded the new mononuclear complex  $[\text{Ru}(\text{trpy})(\text{L}^2-\kappa\text{-N}^2\text{O})] \cdot \text{CH}_3\text{OH} \cdot 2\text{H}_2\text{O}$  [ $\mathbf{2} \cdot \text{CH}_3\text{OH} \cdot 2\text{H}_2\text{O}$ ], where the deprotonated anionic nitrogen of the benzimidazole group coordinated with the metal center. The negative inductive effect of the carboxylate moiety facilitates deprotonation of the benzimidazole NH proton. Molar conductivity measurement confirms the nonelectrolyte nature of the complex in methanol. The complex was characterized by

Scheme 1. Carboxylate/Water Exchange of Complex 2 with Variation of the pH and the Structures below Showing the DFT-Optimized Structures of (Left) 2, (Middle)  $2^{Aq}$ , and (Right)  $2^{Aq}$  at a Singlet Ground State<sup>a</sup>



<sup>a</sup>Color code: Ru, magenta; C, gray; N, blue; O, red; H, white. Hydrogen atoms on the ligand carbon atoms are omitted for clarity.

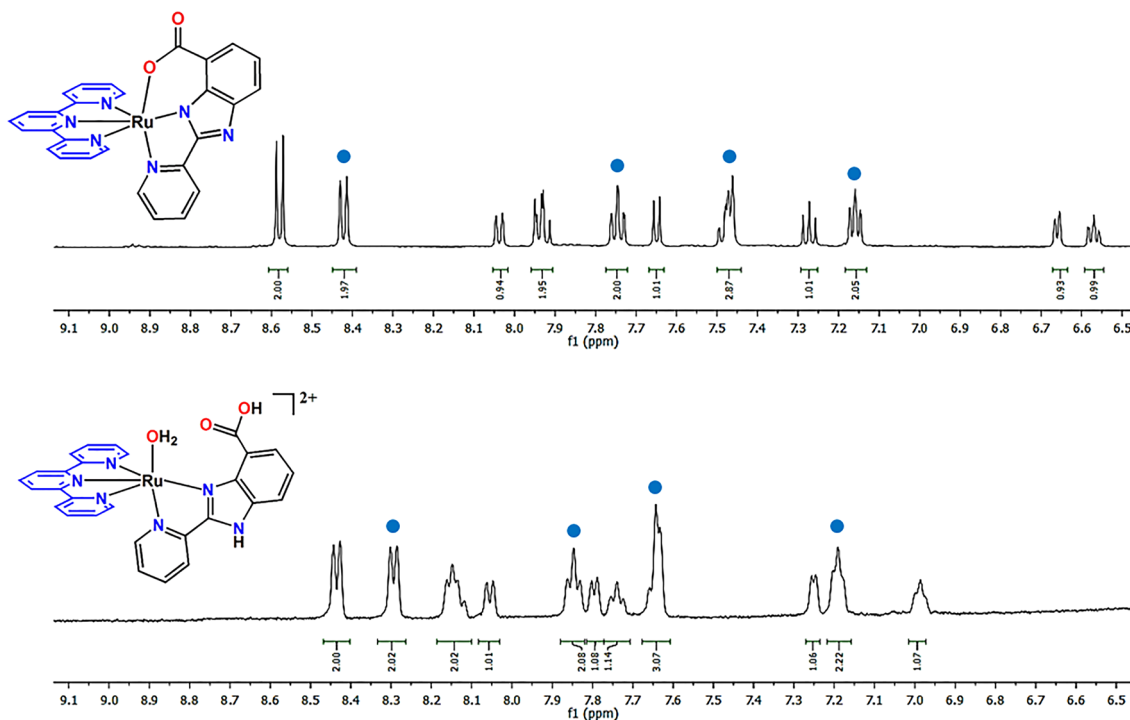


**Figure 2.**  $^1\text{H}$  NMR spectra of 2 in (top)  $\text{CD}_3\text{OD}$  and (bottom) acidic  $\text{D}_2\text{O}/\text{CD}_3\text{OD}$  (4:1, v/v; pD 1.4). The blue circles represent four sets of signals of 2H integration for the trpy ligand.

elemental analysis and by various spectroscopic techniques [electrospray ionization high-resolution mass spectrometry (HRMS-ESI), attenuated-total-reflectance Fourier transform infrared (FTIR-ATR), NMR, and UV-vis]. In the HRMS-ESI(+) spectrum, two peaks at  $m/z$  287.0395 {calcd  $m/z$  287.0346 for  $[2 + 2\text{H}]^{2+}$ } and at  $m/z$  573.0669 {calcd  $m/z$  573.0613 for  $[2 + \text{H}]^+$ } are observed, authenticating formation of the complex (Figure S13). The FTIR-ATR spectrum of a solid sample of 2 shows a strong band at  $1550\text{ cm}^{-1}$  due to the  $\nu(\text{C}=\text{O})_{\text{asym}}$  stretching vibration of the carboxylate group (Figure S14). Notably, the  $\nu(\text{C}=\text{O})_{\text{asym}}$  stretching frequency

of the carboxylate group in complex 2 is red-shifted compared with that of the free  $\text{H}_2\text{L}^2$  ligand ( $1700\text{ cm}^{-1}$ ). This can be accounted for by considering the back-donation of electrons from the ruthenium(II) d orbital to the  $\pi$ -antibonding orbital of the carbonyl group. Because the ruthenium(II) complex is diamagnetic, complex 2 was characterized by 1D and 2D NMR spectroscopy (Figures S15–S17). The  $^1\text{H}$  NMR spectrum of complex 2 in  $\text{CD}_3\text{OD}$  shows 18 proton resonances in the aromatic region. The  $C_s$  symmetry of the complex is indicated by observing four sets of signals of 2H integration for the trpy ligand. Two protons of trpy labeled as proton H5 and H5'

resonate at two different chemical shift values. In the  $^{13}\text{C}$  NMR spectrum, the carbon resonance signal of the carboxylate group is shifted downfield for complex **2** compared to that of the free  $\text{H}_2\text{L}^2$  ligand. This observation indicates coordination of the carboxylate moiety to the ruthenium(II) center, causing a coordination-induced downfield shift. The UV–vis spectrum of **2** in anhydrous methanol is displayed in Figure S18. It shows two types of charge transfer [metal-to-ligand charge transfer (MLCT),  $\text{Ru}(d\pi) \rightarrow \text{ligand}(p\pi^*)$ ; ligand-to-ligand charge transfer (LLCT),  $\text{ligand}(p\pi) \rightarrow \text{ligand}(p\pi^*)$ ] bands.<sup>23,24</sup> The absorption bands at  $\lambda = 234, 275,$  and  $317$  nm are tentatively assigned as LLCT transitions. The MLCT bands are observed at  $\lambda = 346, 362, 503,$  and  $534$  nm.

**Carboxylate Decoordination and Generation of Aqua-Ligated Species  $[\text{Ru}(\text{trpy})(\text{H}_2\text{L}^2-\kappa\text{-N}^2)(\text{OH}_2)]^{2+}$  ( $2^{\text{Aq}}$ ) at pH 1.** To promote water oxidation, the metal complex should have an access of water ligation. For complex **2**, there are two possibilities to generate the catalytically important Ru-aqua species: (i) substitution of the labile carboxylate group by water, and (ii) direct coordination of a water molecule to the metal center to generate a seven-coordinated (CN7) species. The latter possibility is highly unlikely because in the case of **2** a pentagonal-bipyramidal geometry of CN7 species would be highly distorted and sterically hindered. This can be justified if the structural features of  $1^{\text{Aq}}$  are viewed. Although we do not have the X-ray structure of **2**, it can be presumed that complex **2** will have a structural feature similar to that of  $1^{\text{Aq}}$  because both complexes possess a very much comparable ligand environment. In  $1^{\text{Aq}}$ , the bond angles around the ruthenium center in the equatorial plane range from  $78$  to  $101^\circ$ , confirming that a limited space is available for seventh coordination. This is further verified from the DFT-optimized structure of **2** shown in Scheme 1. So, apparently, in the case of **2**, the first option may lead to the generation of a Ru-aqua species. Thummel et al. reported the displacement of carboxylate by water under acidic conditions with the  $[\text{Ru}(\text{trpy})(\text{L})]^+$  complex ( $\text{L} = \text{phenanthroline-2-carboxylate}$ ) to generate a Ru-aqua complex.<sup>16</sup>

The carboxylate/water exchange event of complex **2** was followed spectroscopically under acidic conditions. The FTIR-ATR spectrum of complex **2** in methanol shows a strong band at  $1562\text{ cm}^{-1}$  due to the  $\nu(\text{C}=\text{O})_{\text{asym}}$  stretching vibration of the coordinated carboxylate group. When the solution of complex **2** in methanol is acidified with perchloric acid, the  $\nu(\text{C}=\text{O})_{\text{asym}}$  band is shifted to higher wavenumber ( $1710\text{ cm}^{-1}$ ), indicating that protonation and, consequently, decoordination of the carboxylate group have taken place (Figure S19). This protonation process is also manifested in the  $^1\text{H}$  NMR spectrum of **2** when recorded in acidic  $\text{D}_2\text{O}$  (pD 1.4)/ $\text{CD}_3\text{OD}$  (4:1, v/v). As shown in Figure 2, the proton resonance signals are altered somewhat because of generation of the protonated species  $2^{\text{Aq}}$  (*vide infra*).<sup>16</sup> The  $\text{C}_s$  symmetry is retained in the protonated complex as well because we also observe four similar sets of signals of 2H integration for the trpy ligand.

Further, we followed the proton-induced decoordination events of the carboxylate group by UV–vis spectrophotometry at various pH values. The sample solution of **2** was prepared in aqueous Britton–Robinson (B.–R.) buffer at pH 9.1 containing 20% of  $\text{CF}_3\text{CH}_2\text{OH}$ . The latter was used to dissolve the compound in an aqueous medium. As shown in Figure S20, the spectrum of **2** at pH 9.1 resembles well that obtained from anhydrous methanol (the same numbers of the

MLCT bands), implying that in an aqueous basic medium (pH 9.1) the carboxylate remains coordinated with the ruthenium(II) center. The slight differences in the band positions and intensities that are observed might happen because of the change in the dielectric constant of two different solvents. Upon decreasing the pH gradually by the addition of triflic acid, we observed a color change from red to brown. We also see a change in the MLCT bands by changing the pH from 9.1 to 1.

As can be seen in Figure 3, four MLCT bands at 520, 485, 360, and 340 nm are observed at pH 9.1, whereas at pH 1, only

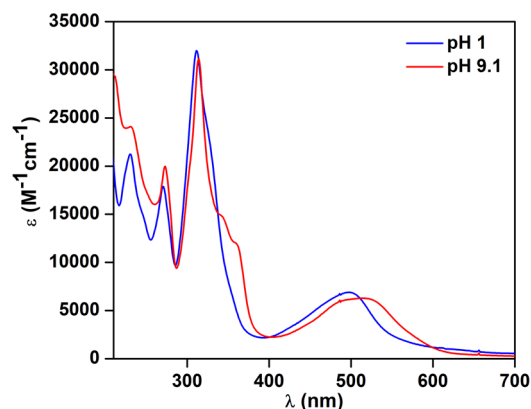


**Figure 3.** UV–vis spectra of **2** measured at (red) pH 9.1 and (blue) pH 1.

one MLCT band at 498 nm is found. This observation can be realized by considering protonation of the ligand  $\text{L}^2$  and consequent carboxylate/water exchange in acidic conditions, which alters the primary coordination sphere of the metal ion. Scheme 1 represents two successive protonation processes at ligand  $\text{L}^2$  and subsequent generation of monoprotinated  $[\text{Ru}(\text{trpy})(\text{HL}^2-\kappa\text{-N}^2)(\text{OH}_2)]^+$  ( $2^{\text{Aq}'}$ ) and double-protonated  $2^{\text{Aq}}$  aqua-ligated species from complex **2**, with a gradual decrease of the pH. In both the  $2^{\text{Aq}'}$  and  $2^{\text{Aq}}$  complexes, the dangling carboxylate/carboxylic group can form a strong intramolecular hydrogen bond with the ligated water molecule, as found in their optimized structures (Scheme 1). The spectroscopic titrations over the pH ranges from 9.1 to 5.0 and from 5.0 to 1.0 are shown in Figures S21a and S22a, respectively. We determined two protonation constants ( $\text{pK}_a$ ) of values 7.8 and 1.5 by sigmoidal fitting of the titration curves shown in Figures S21b and S22b, respectively. The first  $\text{pK}_a$  ( $\text{pK}_a = 7.8$ ) corresponds to protonation of the benzimidazole nitrogen to form the monoprotinated species  $2^{\text{Aq}'}$ , whereas the second  $\text{pK}_a$  ( $\text{pK}_a = 1.5$ ) is assigned for further protonation of the carboxylate to generate  $2^{\text{Aq}}$ . To support these assignments, we further calculated the  $\text{pK}_a$  values of the benzimidazole NH and carboxylic acid group in  $2^{\text{Aq}}$  by DFT calculation. The  $\text{pK}_a$  values are computed to be  $\text{pK}_a^{\text{(NH)}}_{\text{cal}} = 9.02$  and  $\text{pK}_a^{\text{(COOH)}}_{\text{cal}} = 1.22$ . The difference between the experimental and computed values is within the error limit expected for DFT methods.<sup>25a,b</sup> So, it is evident that the double-protonated complex  $2^{\text{Aq}}$  is formed predominantly from **2** under highly acidic conditions (pH 1). The HRMS-ESI(+) spectrum of **2** in an aqueous acidic (pH 1) solution shows a major signal at  $m/z$  287.0345 corresponding to the  $[2^{\text{Aq}} - \text{H}_2\text{O}]^{2+}$  ion (Figure S23), implying the formation of  $2^{\text{Aq}}$  from **2** under acidic conditions. The aqua-ligated complex is able to



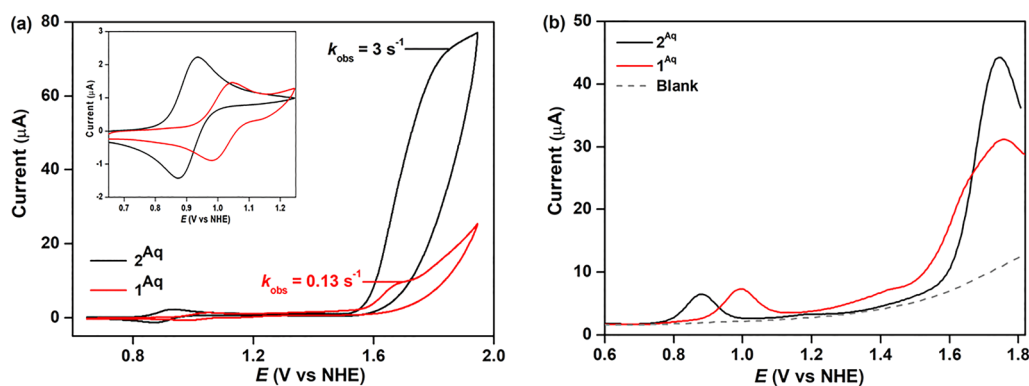


**Figure 4.** Electrochemical behaviors of complexes  $1^{Aq}$  (red line) and  $2^{Aq}$  (black line) in an acidic aqueous solution (pH  $\sim$ 1,  $\text{CF}_3\text{SO}_3\text{H}$ ) containing 20%  $\text{CF}_3\text{CH}_2\text{OH}$ : (a) CV diagrams (background-subtracted); (b) SWV curves. Conditions: [complex] = 1 mM for CV and 0.25 mM for SWV; scan rate of CV = 5 mV/s; for SWV, frequency = 15 Hz and amplitude = 0.025 V; working electrode, glassy carbon.

participate in PCET processes, which facilitate the generation of catalytically active high-valent ruthenium–oxo intermediates at lower potential (*vide infra*).<sup>12,13,17,18,23–25</sup>

**Electrochemical Study.** The redox properties of  $1^{Aq}$  and *in situ* generated  $2^{Aq}$  were analyzed by cyclic voltammetry (CV) and square-wave voltammetry (SWV) in an aqueous triflic acid (pH 1) solution containing 20%  $\text{CF}_3\text{CH}_2\text{OH}$ . All redox potentials were measured with a standard calomel reference electrode and were converted to the normal hydrogen electrode (NHE). The CV and SWV curves of  $1^{Aq}$  and  $2^{Aq}$  are shown in Figure 4. The CV curve of  $1^{Aq}$  shows one reversible oxidation wave along with an electrocatalytic wave at an onset potential of  $\sim$ 1.6 V. The SWV curve of  $1^{Aq}$  exhibits two oxidation peaks at 0.99 and 1.75 V, which are tentatively assigned as the oxidations of  $\text{Ru}^{\text{II}} \rightarrow \text{Ru}^{\text{III}}$  and  $\text{Ru}^{\text{III}} \rightarrow \text{Ru}^{\text{V}}$ , respectively. Similar to  $1^{Aq}$ ,  $2^{Aq}$  also shows one reversible oxidation wave along with a high electrocatalytic wave at an onset potential of  $\sim$ 1.54 V in pH 1. In the SWV curve, the two redox peaks observed at 0.88 and 1.74 V for  $2^{Aq}$  are assigned as the  $\text{Ru}^{\text{II}} \rightarrow \text{Ru}^{\text{III}}$  and  $\text{Ru}^{\text{III}} \rightarrow \text{Ru}^{\text{V}}$  oxidation events, respectively. In both cases, the one-electron nature of the first reversible oxidation wave has been confirmed by controlled potential electrolysis (CPE@1.05 V) analysis, whereas the two-electron nature of the second oxidation event has been apparently assigned based on the Pourbaix diagram (see below). Notably, the  $\text{Ru}^{\text{III}}/\text{Ru}^{\text{II}}$  redox potential of  $2^{Aq}$  (0.88 V) at pH 1 is 100 mV lower than that of  $1^{Aq}$  (0.99 V). In complex  $2^{Aq}$ , the dangling  $-\text{CO}_2\text{H}$  group most likely involves a strong intramolecular hydrogen-bonding interaction with the coordinated water molecule, which might facilitate the removal of proton from water via a PCET process during oxidation to the  $\text{Ru}^{\text{III}}$  state. On the other hand, the oxidation potential for the formation of formal  $\text{Ru}^{\text{V}}$  species is only 10 mV lower. For both complexes, the potential for  $\text{Ru}^{\text{V}}$  generation lies in the onset of the catalytic wave, suggesting that the high-valent formal  $\text{Ru}^{\text{V}}$  triggers the water oxidation reaction. The higher electrocatalytic current of  $2^{Aq}$  compared to that of  $1^{Aq}$  observed in the CV diagram at pH 1 confirms the superior catalytic activity of  $2^{Aq}$  toward water oxidation, implying that the dangling carboxylic group plays a vital role in boosting the water oxidation reaction (*vide infra*). However, it should be noted that we observed a lower intensity of the electrocatalytic current with complex **2** at neutral-to-basic pH conditions compared to pH 1 (Figure S24). This phenomenon is attributed to the shifting of equilibrium from the catalytically

active form  $2^{Aq}$  to the inactive form **2** by changing the pH from highly acidic to basic conditions ( $2^{Aq} \rightarrow \mathbf{2}$ ).

To gain more comprehensive insights into the various redox compositions generated during oxidation, we studied the electrochemical behavior of complex  $1^{Aq}$  and the Ru-aqua species derived from **2** as a function of the pH in a B.–R. buffer aqueous solution containing 20%  $\text{CF}_3\text{CH}_2\text{OH}$ . The Pourbaix diagrams of both of the complexes are depicted in Figure 5. The redox potentials were measured by SWV (Figures S25 and S26) and are represented in Figure 5. Interestingly, we observe two distinct Pourbaix diagrams, even

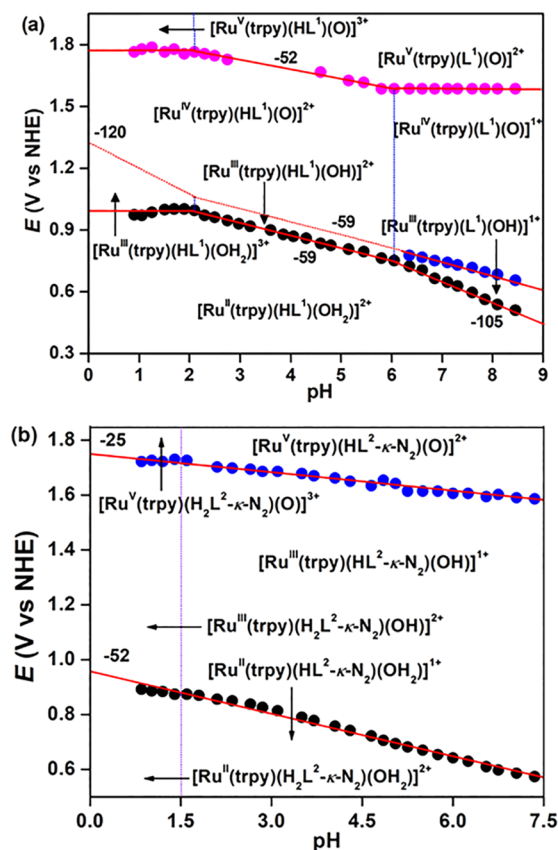


**Figure 5.** Pourbaix diagrams of (a) complex  $1^{Aq}$  and (b) the Ru-aqua species derived from **2**.

**Table 1. Redox Potentials and Catalytic Data for the Present Ru-OH<sub>2</sub> Complexes and the Related Complexes Reported in the Literature at pH ~1**

entry	complex <sup>a</sup>	E <sub>1/2</sub> (V) vs NHE			TOF <sub>i</sub> <sup>b</sup>	k <sub>obs</sub> <sup>c</sup> [TOF <sub>max</sub> ] <sup>d</sup>	ref
		III/II	IV/III	V/IV [V/III]			
1	[Ru(trpy)(HL <sup>1</sup> )(OH <sub>2</sub> )] <sup>2+</sup> ( <b>1</b> <sup>Aq</sup> )	0.99	1.18 <sup>e</sup>	1.75 <sup>e</sup>	0.014	0.13	this work
2	[Ru(trpy)(H <sub>2</sub> L <sup>2-κ-N<sup>2</sup></sup> )(OH <sub>2</sub> )] <sup>2+</sup> ( <b>2</b> <sup>Aq</sup> )	0.88		[1.74]	0.3	3	this work
3	[Ru(trpy)(bpy)(OH <sub>2</sub> )] <sup>2+</sup>	1.06	1.22	1.92	0.01		24
4	[Ru(trpy)(phenCO <sub>2</sub> )] <sup>+</sup>				0.15		16
5	[Ru(trpy)(Mebim-py)(OH <sub>2</sub> )] <sup>2+</sup>	1.12	1.48	1.65		2	26
6	[Ru(trpy)(phenSO <sub>3</sub> )] <sup>+</sup>	1.11			0.88	1350	15
7	<i>cis</i> -[Ru(trpy)(qc)(OH <sub>2</sub> )] <sup>+</sup>	0.82		1.71		[6.8]	17
8	<i>trans</i> -[Ru(trpy)(qc)(OH <sub>2</sub> )] <sup>+</sup>	0.67	1.20	1.62	0.68	[4.2]	17
9	<i>cis</i> -[Ru(trpy)(pic)(OH <sub>2</sub> )] <sup>+</sup>	0.86	1.31	1.67	0.11	[0.3]	17
10	<i>trans</i> -[Ru(trpy)(pic)(OH <sub>2</sub> )] <sup>+</sup>	0.76	1.09	1.60	0.24	[1.2]	17

<sup>a</sup>Ligand abbreviations: trpy = 2,2':6',2''-terpyridine, bpy = 2,2'-bipyridine, phenCO<sub>2</sub> = 1,10-phenanthroline-2-carboxylate, Mebim-py = 3-methyl-1-pyridylbenzimidazol-2-ylidene, phenSO<sub>3</sub> = 1,10-phenanthroline-2-sulfonate, qc = 8-quinolinecarboxylate, and pic = 2-picolate. <sup>b</sup>Initial turnover frequency (s<sup>-1</sup>). These values are determined from Ce<sup>IV</sup>-driven catalytic reactions at pH 1. <sup>c</sup>Electrocatalytic rate constant (s<sup>-1</sup>) at pH 1. <sup>d</sup>Maximum turnover frequency (s<sup>-1</sup>). These values are estimated from the foot of the wave analysis at pH 1. <sup>e</sup>Estimated from the Pourbaix diagram shown in Figure Sa.

though the complexes have comparable coordination environments, implying that they are electronically different.

For **1**<sup>Aq</sup>, the diagram indicates that at a Ru<sup>II</sup> state the complex exists as [Ru<sup>II</sup>(trpy)(HL<sup>1</sup>)(OH<sub>2</sub>)]<sup>2+</sup> in the entire range of 0.85 ≤ pH ≤ 8.45. The Ru<sup>III</sup>/Ru<sup>II</sup> couple shows three different slopes over three pH regions. In the pH range from 0.85 to 2.10, the Ru<sup>III</sup>/Ru<sup>II</sup> potential remains pH-independent, implying only electron transfer for the [Ru<sup>III</sup>(trpy)(HL<sup>1</sup>)(OH<sub>2</sub>)]<sup>3+</sup>/[Ru<sup>II</sup>(trpy)(HL<sup>1</sup>)(OH<sub>2</sub>)]<sup>2+</sup> couple. From pH 2.1 to 6.05, the Ru<sup>III</sup>/Ru<sup>II</sup> potential decreases linearly with a slope of -59 mV/pH, consistent with a one-electron and one-proton (1e<sup>-</sup>, 1H<sup>+</sup>) PCET process for the [Ru<sup>III</sup>(trpy)(HL<sup>1</sup>)(OH)]<sup>2+</sup>/[Ru<sup>II</sup>(trpy)(HL<sup>1</sup>)(OH<sub>2</sub>)]<sup>2+</sup> redox couple. Thus, the pK<sub>a</sub> value of [Ru<sup>III</sup>(trpy)(HL<sup>1</sup>)(OH<sub>2</sub>)]<sup>3+</sup> was determined to be 2.10, which is comparable to those of other reported "Ru<sup>III</sup>-OH<sub>2</sub>" species.<sup>17,23,24</sup> At the higher region 6.05 ≤ pH ≤ 8.45, the Ru<sup>III</sup>/Ru<sup>II</sup> redox potential decreases linearly with a slope of -105 mV/pH, reflecting a one-electron and two-proton (1e<sup>-</sup>, 2H<sup>+</sup>) PCET process for the redox couple [Ru<sup>III</sup>(trpy)(L<sup>1</sup>)(OH)]<sup>+</sup>/[Ru<sup>II</sup>(trpy)(HL<sup>1</sup>)(OH<sub>2</sub>)]<sup>2+</sup>. Here, the sources of the two protons might be one from ligand HL<sup>1</sup> and another from the coordinated water. The Ru<sup>IV</sup>/Ru<sup>III</sup> redox response was only observed beyond pH 6.05. Between pH 0.85 and 6.05, we did not observe the corresponding redox wave probably because of the slow kinetics of electron and proton transfer at the electrode surface. However, the observed points can be rationally extrapolated, as shown in the diagram. Between pH 0.85 and 2.10, we assume a slope of -120 mV/pH for the (1e<sup>-</sup>, 2H<sup>+</sup>) PCET process to generate [Ru<sup>IV</sup>(trpy)(HL<sup>1</sup>)(=O)]<sup>2+</sup> from [Ru<sup>III</sup>(trpy)(HL<sup>1</sup>)(OH<sub>2</sub>)]<sup>3+</sup>. We obtain a slope of -59 mV/pH in the range of pH 2.1–8.45. Therefore, we assign the redox couple in the region 2.10 ≤ pH ≤ 6.05 to [Ru<sup>IV</sup>(trpy)(HL<sup>1</sup>)(=O)]<sup>2+</sup>/[Ru<sup>III</sup>(trpy)(HL<sup>1</sup>)(OH)]<sup>2+</sup>, whereas the redox couple in the range 6.05 ≤ pH ≤ 8.45 is assigned to [Ru<sup>IV</sup>(trpy)(L<sup>1</sup>)(=O)]<sup>2+</sup>/[Ru<sup>III</sup>(trpy)(L<sup>1</sup>)(OH)]<sup>+</sup>. The oxidation potential to generate ruthenium(V) species is found to be pH-independent in the pH ranges from 0.85 to 2.10 and from 6.05 to 8.45, whereas the potential decreases linearly with a slope of -52 mV/pH from pH 2.10 to 6.05. Thus, the redox couples in the regions 0.85 ≤ pH ≤ 2.10, 2.10 ≤ pH ≤ 6.05, and 6.05 ≤ pH ≤ 8.45 can be assigned to [Ru<sup>V</sup>(trpy)(HL<sup>1</sup>)(=O)]<sup>3+</sup>/[Ru<sup>IV</sup>(trpy)(HL<sup>1</sup>)(=O)]<sup>2+</sup>,

[Ru<sup>V</sup>(trpy)(L<sup>1</sup>)(=O)]<sup>3+</sup>/[Ru<sup>IV</sup>(trpy)(HL<sup>1</sup>)(=O)]<sup>2+</sup>, and [Ru<sup>V</sup>(trpy)(L<sup>1</sup>)(=O)]<sup>2+</sup>/[Ru<sup>IV</sup>(trpy)(L<sup>1</sup>)(=O)]<sup>+</sup>, respectively.

The electrochemical studies with complex **2** over the pH range 0.85–7.35 reveal two types of PCET processes for two oxidation steps. The PCET events clearly indicate the generation of Ru-aqua species from **2** via proton-induced carboxylate/water exchange in the specified pH region. From the pK<sub>a</sub> values of benzimidazole NH and carboxylic acid (pK<sub>a</sub><sup>(NH)</sup><sub>expt</sub> = 7.8 and pK<sub>a</sub><sup>(COOH)</sup><sub>expt</sub> = 1.5), it is evident that at a Ru<sup>II</sup> state the aqua-ligated complex exists in two different protonated forms, giving rise to species **2**<sup>Aq</sup> in the region 0 ≤ pH ≤ 1.5 and **2**<sup>Aq'</sup> in the region 1.5 ≤ pH ≤ 7.8. As shown in the diagram, the first Ru<sup>III</sup>/Ru<sup>II</sup> potential decreases linearly with the pH over the entire pH range with a slope of -53 mV/pH, implying a (1e<sup>-</sup>, 1H<sup>+</sup>) PCET process. So, we tentatively assign the redox couple in the region 0.85 ≤ pH ≤ 1.5 to [Ru<sup>III</sup>(trpy)(H<sub>2</sub>L<sup>2-κ-N<sup>2</sup></sup>)(OH)]<sup>2+</sup> (**2**<sup>OH</sup>)/[Ru<sup>II</sup>(trpy)(H<sub>2</sub>L<sup>2-κ-N<sup>2</sup></sup>)(OH<sub>2</sub>)]<sup>2+</sup> (**2**<sup>Aq</sup>), whereas the redox couple in the range 1.5 ≤ pH ≤ 7.35 is assigned to [Ru<sup>III</sup>(trpy)(HL<sup>2-κ-N<sup>2</sup></sup>)(OH)]<sup>+</sup> (**2**<sup>OH'</sup>)/[Ru<sup>II</sup>(trpy)(HL<sup>2-κ-N<sup>2</sup></sup>)(OH<sub>2</sub>)]<sup>+</sup> (**2**<sup>Aq'</sup>). On the other hand, the second oxidation potential decreases linearly with a slope of -25 mV/pH over the whole pH range. This phenomenon can be ascribed as a two-electron and one-proton (2e<sup>-</sup>, 1H<sup>+</sup>) PCET process for the formal [Ru<sup>V</sup>(trpy)(H<sub>2</sub>L<sup>2-κ-N<sup>2</sup></sup>)(=O)]<sup>3+</sup> (**2**<sup>oxo</sup>)/**2**<sup>OH</sup> and [Ru<sup>V</sup>(trpy)(HL<sup>2-κ-N<sup>2</sup></sup>)(=O)]<sup>2+</sup> (**2**<sup>oxo'</sup>)/**2**<sup>OH'</sup> redox couples in the regions of 0.85 ≤ pH ≤ 1.5 and 1.5 ≤ pH ≤ 7.35, respectively. Furthermore, we calculated the redox potentials of the **2**<sup>OH</sup>/**2**<sup>Aq</sup> and **2**<sup>oxo</sup>/**2**<sup>OH</sup> couples by DFT calculation at pH 1. The calculated potential<sup>25a–c</sup> values [E<sub>1/2</sub><sup>III/II</sup><sub>cal</sub> = 0.93 V vs NHE (**2**<sup>OH</sup>/**2**<sup>Aq</sup>); E<sub>1/2</sub><sup>V/III</sup><sub>cal</sub> = 1.62 V vs NHE (**2**<sup>oxo</sup>/**2**<sup>OH</sup>)] are in well agreement with the experimental values [E<sub>1/2</sub><sup>III/II</sup><sub>expt</sub> = 0.88 V vs NHE (**2**<sup>OH</sup>/**2**<sup>Aq</sup>); E<sub>1/2</sub><sup>V/III</sup><sub>expt</sub> = 1.74 V vs NHE (**2**<sup>oxo</sup>/**2**<sup>OH</sup>)], supporting the assignments of species at pH 1. The redox potentials of the two Ru-aqua complexes (**1**<sup>Aq</sup> and **2**<sup>Aq</sup>) at pH 1 are summarized in Table 1 along with other relevant ruthenium complexes previously reported in the literature.

**Spectroscopic Redox Titration.** The redox titrations of both complexes **1**<sup>Aq</sup> and **2**<sup>Aq</sup> were performed with ceric ammonium nitrate (CAN) in an aqueous 0.1 M CF<sub>3</sub>SO<sub>3</sub>H solution (pH 1) containing 20% CF<sub>3</sub>CH<sub>2</sub>OH to detect various

intermediates formed upon oxidation. The titration was followed by UV–vis spectrophotometry. The spectral changes of  $1^{Aq}$  and  $2^{Aq}$  at different oxidation states in pH 1 are shown in Figures S27 and 6, respectively. For  $1^{Aq}$ , upon the successive

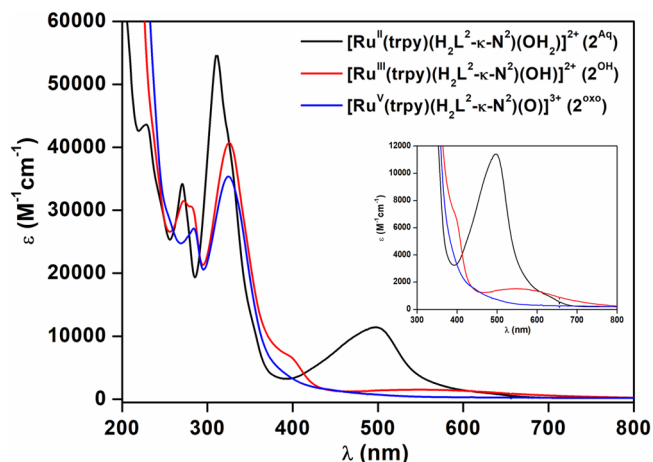
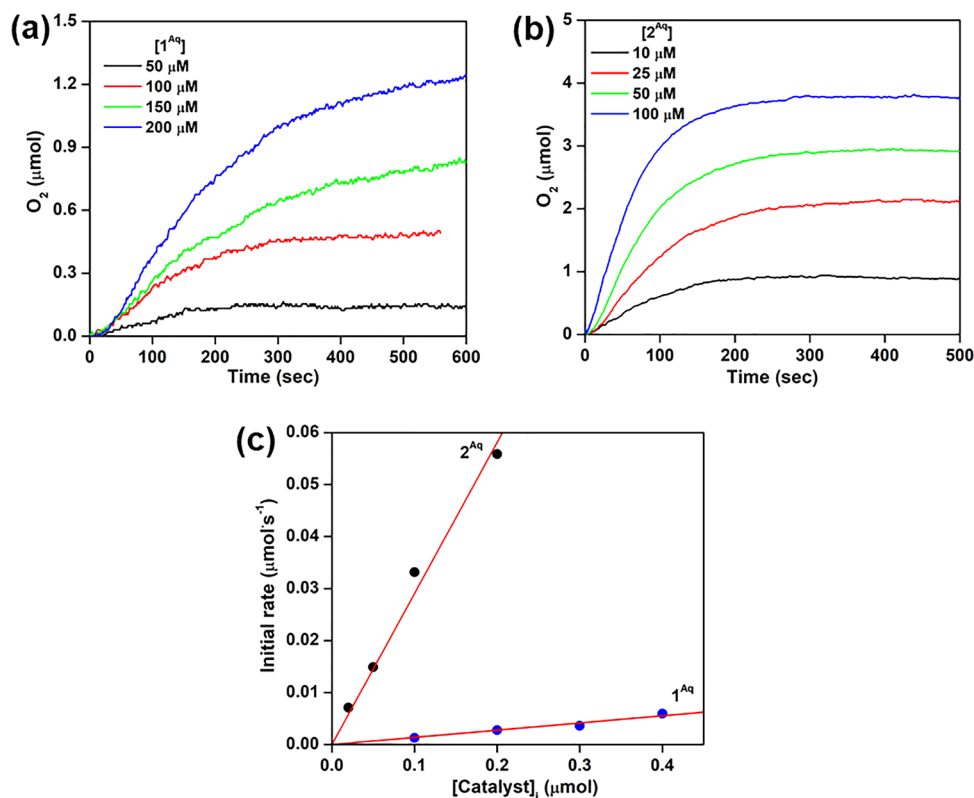


**Figure 6.** UV–vis spectra of  $2^{Aq}$  at different formal oxidation states generated from stoichiometric oxidation with  $Ce^{IV}$  in a pH  $\sim 1$  aqueous  $CF_3SO_3H$  solution containing 20%  $CF_3CH_2OH$ .

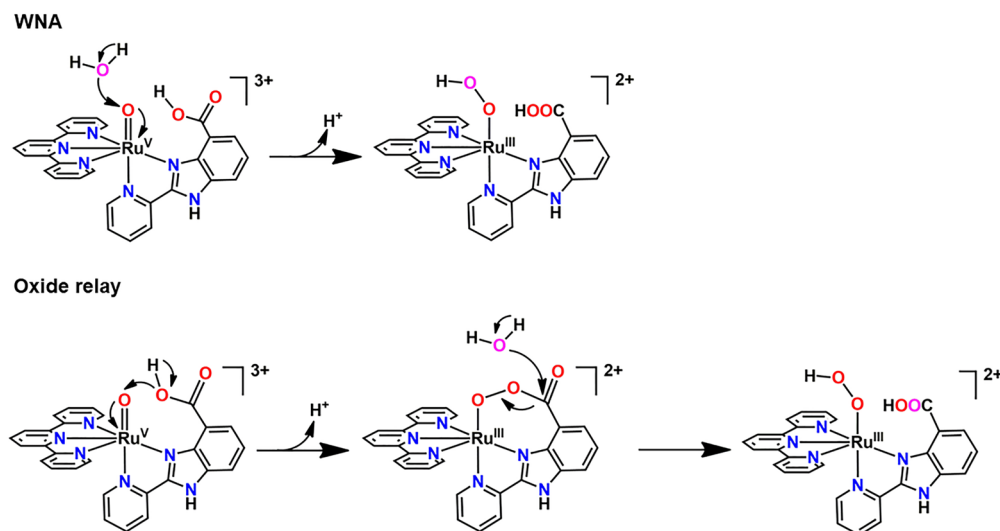
addition of up to 1 equiv of CAN to the  $Ru^{II}$  state, the intensities of the  $\pi \rightarrow \pi^*$  band at 312 nm decrease steadily and the band position gradually shifts to 323 nm. The intensities of the MLCT band at 487 nm also decrease steadily. The finding of isosbestic points at  $\lambda = 275, 290, 325,$  and  $395$  nm indicates

a clean transformation from the  $Ru^{II}$  to  $Ru^{III}$  state (Figure S28a). The addition of 1 equiv more of CAN to  $Ru^{III}$  causes the lowering of the band intensity at 323 nm, and the MLTC band at 487 nm becomes almost featureless (Figure S28b). This observation can be correlated with the conversion of the  $Ru^{III}$  state to the  $Ru^{IV}$  state, as is evident from the titration curve shown in Figure S28c. Upon further addition of CAN, however, no significant changes in the absorption spectra were observed, probably because of its rapid consumption for the oxidation of water. Therefore, from the redox titration, it is obvious that complex  $1^{Aq}$  undergoes two successive one-electron oxidations to generate  $Ru^{III}$  and  $Ru^{IV}$  intermediates, respectively. These findings support the formation of various oxidation states as described in the Pourbaix diagram of  $1^{Aq}$ , particularly at pH 1.

In the case of  $2^{Aq}$ , with the incremental addition of up to 1 equiv of CAN to  $Ru^{II}$ , the intensities of the  $\pi \rightarrow \pi^*$  band at 310 nm decrease progressively and the band position gradually shifts to 325 nm, similar to  $1^{Aq}$ . The intensities of the MLCT band at 498 nm decrease steadily, while two new low-intensity LMCT bands at 400 and 530 nm develop (Figure S29a). This phenomenon can be attributed with generation of the  $Ru^{III}$  state. The oxidation of  $Ru^{II}$  to  $Ru^{III}$  happens in a single step, as is evident from the isosbestic points at  $\lambda = 273, 290, 325,$  and  $413$  nm. Upon the addition of 2 equiv more of CAN to the  $Ru^{III}$  state, the intensities of the bands at 325, 400, and 530 nm decrease progressively (Figure S29b). Further additions of CAN do not significantly alter the spectral features. This can apparently be ascribed to the formation of a  $Ru^{IV}$  intermediate (Figure S29c). Therefore, complex  $2^{Aq}$  undergoes one- and two-electron oxidations successively to formally generate  $Ru^{III}$



**Figure 7.** Oxygen evolution profiles at various concentrations of catalyst: (a) for  $1^{Aq}$  and (b) for  $2^{Aq}$ . Conditions: a pH 1  $CF_3SO_3H$  solution with 20%  $CF_3CH_2OH$  (total volume 2 mL);  $[CAN] = 100$  mM;  $T = 298$  K. (c) Plots of the initial rate of  $O_2$  production versus the amount of complexes  $1^{Aq}$  (blue circles) and  $2^{Aq}$  (black circles).

Scheme 2. Plausible O–O Bond Formation Pathway with  $2^{Aq}$ 

and  $Ru^V$  intermediates, respectively. Thus, for complex  $2^{Aq}$ ,  $Ru^{IV}$  seems to be a missing oxidation state, consistent with the Pourbaix diagram as stated above.

**Water Oxidation Catalysis.** The oxidation of water to dioxygen ( $O_2$ ) catalyzed by  $1^{Aq}$  and  $2^{Aq}$  was investigated in the presence of CAN as a sacrificial oxidant in an aqueous 0.1 M  $CF_3SO_3H$  (pH  $\sim 1$ ) solution containing 20%  $CF_3CH_2OH$ . Complex  $2^{Aq}$  was generated *in situ* by dissolving complex **2** in an aqueous acidic solvent, considering 100% conversion. The oxygen evolution was monitored by a differential pressure manometer, and the presence of  $O_2$  was identified by an oxygen sensor at the end of the measurement. The oxygen evolution kinetics were studied at various concentrations of both catalysts (10–200  $\mu M$ ) containing excess CAN (100 mM) at 25  $^\circ C$ . The oxygen evolution curves catalyzed by  $1^{Aq}$  and  $2^{Aq}$  are shown in parts a and b of Figure 7, respectively. The initial rates of oxygen evolution are calculated from the initial slope and plotted against  $[catalyst]_i$ , as shown in Figure 7c. In each case, the initial rate values increase linearly with  $[catalyst]_i$ , suggesting a unimolecular reaction. The first-order dependence with respect to  $[catalyst]_i$  implies that only one molecule of the complex is involved in the rate-determining step. The initial turnover frequencies ( $TOF_i$ ) for  $1^{Aq}$  and  $2^{Aq}$  were calculated from the slope as 0.014 and 0.3  $s^{-1}$ , respectively. The rate constant of  $2^{Aq}$  is remarkably higher ( $\sim 21$  times) than that of  $1^{Aq}$  (see Table 1 for a comparison with other related reported compounds). Although we could achieve a higher  $TOF_i$  for  $2^{Aq}$ , the catalytic performance is limited to moderate turnovers. Using  $[complex]/[CAN] = 50 \mu M/100 \text{ mM}$ , we could achieve only a few turnover numbers ( $TON = 2$  for  $1^{Aq}$  and 30 for  $2^{Aq}$ ), suggesting that both complexes suffered from degradation under highly oxidizing  $Ce^{IV}$  conditions. Nevertheless, the presence of a  $-CO_2H$  moiety increases the robustness of  $2^{Aq}$  rather than  $1^{Aq}$ . In an electrochemical study, we also observed a much higher catalytic current for  $2^{Aq}$  than  $1^{Aq}$ , as shown in Figure 4a. From an electrochemical study, we estimated the  $k_{obs}$  values of  $0.13 \pm 0.02 \text{ s}^{-1}$  for  $1^{Aq}$  and  $3.00 \pm 0.10 \text{ s}^{-1}$  for  $2^{Aq}$  at pH 1 (for details, see Figures S30–S35 and Table S3). Here also we found a remarkably higher  $k_{obs}$  value for  $2^{Aq}$  than  $1^{Aq}$  (Table 1). Given the similar primary coordination environments in both complexes, the above results point toward the fact that

the dangling  $-CO_2H$  group must be involved in fine-tuning of the secondary coordination sphere to reduce the activation energy barrier in the rate-limiting step. The presence of a pendant carboxylic side arm in complex  $2^{Aq}$  can stabilize the high-valent states of the complex or various other intermediates through intramolecular hydrogen-bonding interaction.<sup>13</sup> Moreover, it may participate in O–O bond formation, promoting an oxide relay mechanism (*vide infra*).<sup>20</sup> Therefore, the presence of dangling  $-CO_2H$  in  $2^{Aq}$  enhances the reaction rate, whereas the absence of a carboxylic moiety in  $1^{Aq}$  makes the catalyst inefficient.

**Mechanism of O–O Bond Formation in  $2^{Aq}$ .** The observed first-order dependence of the reaction rate with respect to the catalyst concentrations implies a WNA mechanism for the O–O bond formation step, as was mostly reported in the literature for other related ruthenium complexes.<sup>5,6</sup> Scheme 2 shows two possible pathways for the O–O coupling step with complex  $2^{Aq}$ . In a familiar WNA pathway, water can attack directly at the oxo center of the  $Ru^V=O$  unit to form the O–O bond. In another pathway, instead of a direct water attack at the  $Ru^V=O$  center, the oxygen of a pendant carboxylic group can first react with the oxo moiety to form a O–O bond, followed by WNA at the electrophilic carbon atom of the formed percarboxylate, referred to as an oxide relay mechanism.<sup>20</sup>

To verify the reaction pathway, we performed a catalytic reaction using  $^{18}O$ -labeled water under one turnover condition. In a typical experiment, complex **2** was dissolved in 100  $\mu L$  of  $CF_3CH_2OH$  containing 20  $\mu L$  of neat triflic acid, and to it was added 4 equiv of CAN dissolved in 380  $\mu L$  of 97%  $H_2^{18}O$  to initiate the catalytic reaction. A similar experiment was also performed using  $H_2^{16}O$  instead of  $^{18}O$ -labeled water. At the end of the reaction, the solvent was removed from each reaction to obtain solid samples that were analyzed by HRMS-ESI(+), FTIR-ATR, and resonance Raman spectroscopy.

The HRMS-ESI(+) spectrum of the sample obtained from the catalytic reaction in  $H_2^{16}O$  exhibits a peak corresponding to  $[Ru(trpy)(HL^2-\kappa-N^2)]^+$  species at  $m/z$  573.0608, which is nearly two-mass-unit-upshifted to  $m/z$  575.0698 for the sample obtained from the reaction using  $^{18}O$ -labeled water (Figure S36). The experimental isotope pattern of the  $^{18}O$ -labeled sample is an overlapping signal of unlabeled and labeled



complexes. The isotope pattern is successfully simulated with a percentage ratio of  $[\text{Ru}(\text{trpy})(\text{HL}^2\text{-}\{^{16}\text{O}^{16}\text{O}\})]^+ : [\text{Ru}(\text{trpy})(\text{HL}^2\text{-}\{^{16}\text{O}^{18}\text{O}\})]^+ : [\text{Ru}(\text{trpy})(\text{HL}^2\text{-}\{^{18}\text{O}^{18}\text{O}\})]^+ = 30:51:19$ . So, mass analysis clearly indicates that the oxygen atom of the water molecule is incorporated into the carboxylic moiety during the catalytic process. In the FTIR-ATR spectra, as shown in Figure 8, the  $\nu(\text{C}=\text{O})_{\text{asym}}$  vibration of the

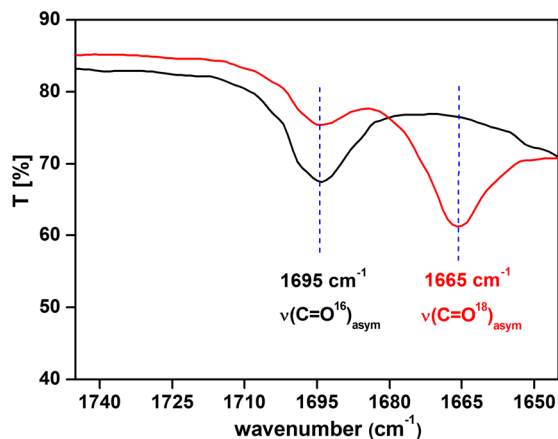


**Figure 8.** FTIR-ATR spectra of samples obtained after **2** was treated with 4 equiv of CAN using (black line)  $^{16}\text{O}$ -labeled and (red line)  $^{18}\text{O}$ -labeled water (acidic pH).

dangling carboxylic group for the unlabeled sample appears at  $1695\text{ cm}^{-1}$ , whereas this stretching vibration appears at the lower wavenumber  $1665\text{ cm}^{-1}$  in the  $^{18}\text{O}$ -labeled sample (see Figure S37 for the full-range spectra). The observed isotopic shift of  $\Delta\nu_{\text{obs}} = 30\text{ cm}^{-1}$  is consistent with the calculated isotopic shift value  $\Delta\nu_{\text{cal}} = 34\text{ cm}^{-1}$ , confirming incorporation of the heavier oxygen isotope into the carboxylic moiety under catalytic conditions. Similarly, in resonance Raman spectroscopy with excitation at  $512\text{ nm}$ , we observed an isotopic shift of  $\Delta\nu_{\text{obs}} = 30\text{ cm}^{-1}$  upon  $^{18}\text{O}$  labeling in the  $\nu(\text{C}=\text{O})_{\text{sym}}$  vibration (Figure S38). A controlled labeling experiment without the addition of CAN showed that no  $^{18}\text{O}$  exchange occurred at all between water and  $-\text{CO}_2\text{H}$  for at least 6 h. These findings undoubtedly validate the oxide relay pathway, where WNA takes place at the carbon center of the percarboxylate group instead of a direct attack at the oxo of

the formal  $\text{Ru}^{\text{V}}=\text{O}$  unit (Scheme 2). As can be seen from the DFT-optimized structure of the formal  $2^{\text{oxo}}$  species at the quartet ground state shown in Figure 9a, the oxygen atoms of the pendant carboxylic group are positioned within a bonding distance of around  $3.024\text{ \AA}$  (average distance) from the reactive oxo center of the  $\text{Ru}^{\text{V}}=\text{O}$  unit. Such a close proximity can be anticipated to facilitate the intramolecular O–O bond formation between the oxo and an oxygen atom of the carboxylic group.

In  $2^{\text{oxo}}$ , the quartet and doublet states are close to degenerate. The ground quartet state is only  $1.25\text{ kcal/mol}$  lower in energy than the doublet state. The Mulliken spin-density plots of both states are depicted in Figure S39. The electronic structure of  $2^{\text{oxo}}$  at the quartet ground state can be described as  $[\text{Ru}^{\text{III}}(\text{trpy})(\text{H}_2\text{L}^2\text{-}\kappa\text{-N}^2)^+\text{(O}^{\bullet-})]^{3+}$ , featuring a low-spin  $\text{Ru}^{\text{III}}$  center ( $S = 1/2$ ) ferromagnetically coupled with an oxyl radical ( $S = 1/2$ ) and a  $\text{H}_2\text{L}^2$  ligand-based cation radical ( $S = 1/2$ ). While the basicity of the carboxylic group is largely reduced at acidic pH, the highly reactive oxyl group<sup>27</sup> might provoke O–H bond cleavage of the  $-\text{COOH}$  group and promote O–O bond formation via a radical coupling pathway. During the O–O bond formation step, the electron from  $\text{H}^{\bullet}$  is formally transferred to the cationic-radicaloid benzimidazole moiety of the ligand along with the release of a proton to generate a putative doublet ruthenium(III) percarboxylate (**3**) intermediate. The DFT-optimized structure and spin-density plot for **3** are shown in Figures 9b and S40, respectively. The O–O bond distance ( $1.451\text{ \AA}$ ) of the calculated structure of **3** is in agreement with the characteristic metal–peroxo complex. The carbon atom of the percarboxylate intermediate is electrophilic in nature with a partial positive charge of  $+0.39$ . This makes the WNA at the carbon center favorable. In the proceeding steps, once the water has attacked the electrophilic carbon, breaking of the C–O bond would take place readily to form a putative ruthenium(III) hydroperoxo intermediate (**4**) that undergoes further proton-coupled oxidation to release  $\text{O}_2$ . The solvent kinetic isotope effect value was determined to be 2.00 by comparing the CV curves of  $2^{\text{Aq}}$  in  $\text{H}_2\text{O}$  (pH 1) and  $\text{D}_2\text{O}$  (pD 1.4), as shown in Figure S41. This result indicates that the rate-determining step is associated with cleavage of the O–H bond, which most probably occurs either during the O–O bond formation step ( $2^{\text{oxo}} \rightarrow \mathbf{3}$ ) or during the WNA step at the carbon center of the percarboxylate ( $\mathbf{3} \rightarrow \mathbf{4}$ ). Further computational studies should allow us to acquire detailed

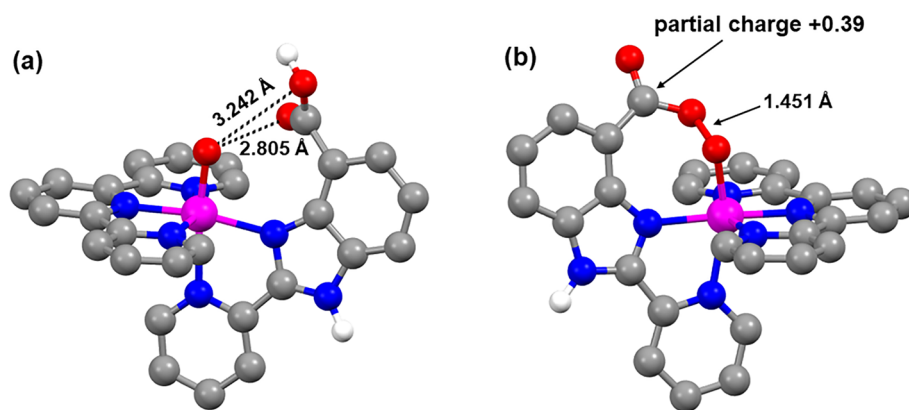


**Figure 9.** DFT-optimized structures of (a) quartet  $2^{\text{oxo}}$  and (b) doublet ruthenium(III) percarboxylate intermediate (**3**) derived from  $2^{\text{Aq}}$  during the catalytic process. Color code: Ru, magenta; C, gray; N, blue; O, red; H, white. Hydrogen atoms on the ligand carbon atoms are omitted for clarity.

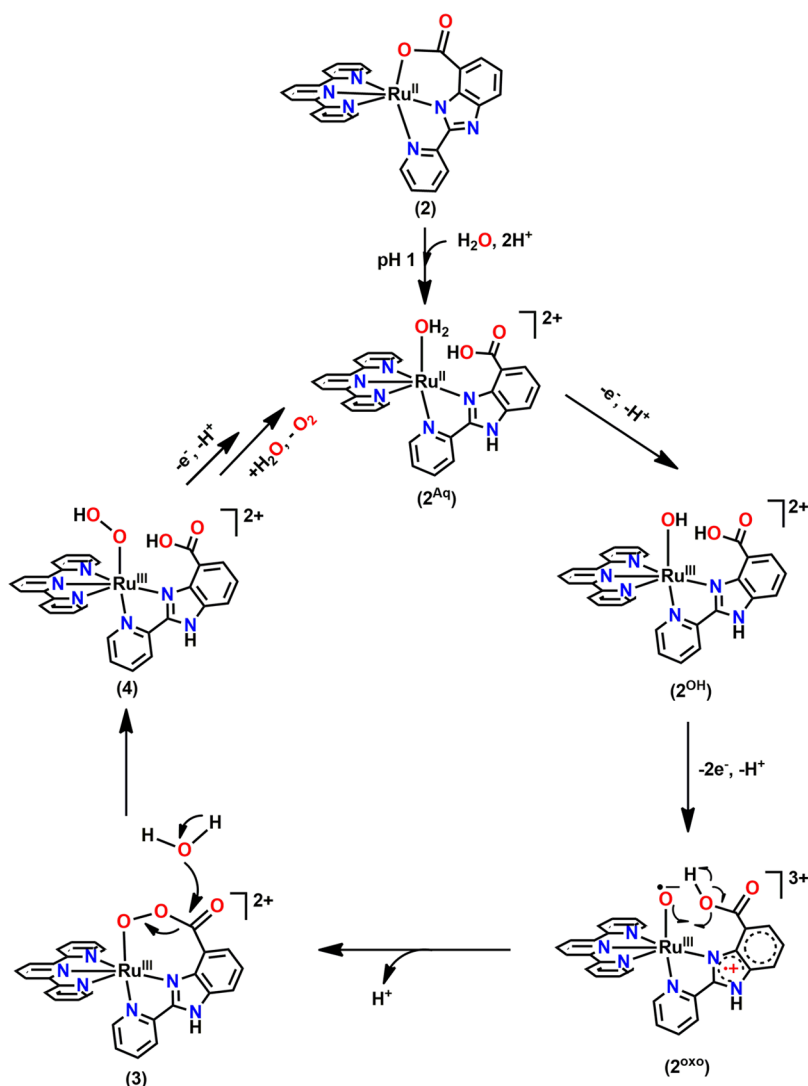


**Figure 10.** Plausible reaction pathway for water oxidation mediated by **2** at pH 1.

mechanistic information. So, on the basis of the experimental as well as preliminary computational studies discussed above, we propose a plausible reaction pathway for water oxidation mediated by **2** at pH 1, as shown in Figure 10.

## CONCLUSIONS

In this work, we have reported the synthesis and characterizations of a new ruthenium(II) complex **2** along with a previously reported aqua-coordinated complex **1**<sup>Aq</sup>. In an acidic aqueous medium (pH 1), complex **2** undergoes protonation-induced carboxylate/water exchange to produce catalytically important aqua-ligated complex **2**<sup>Aq</sup>. Here we have demonstrated the effect of a dangling carboxylic group toward the water oxidation reactivity by comparing the catalytic performances of **1**<sup>Aq</sup> and **2**<sup>Aq</sup>. The catalytic rates for **1**<sup>Aq</sup> and **2**<sup>Aq</sup> were determined from the chemically induced reaction as well as from the electrocatalytic current at pH 1. Complex **2**<sup>Aq</sup> shows a several times higher catalytic rate than complex **1**<sup>Aq</sup>. The dangling carboxylic group in **2**<sup>Aq</sup> enhances the rate of reaction enormously by participating in the O–O bond formation reaction, where instead of the direct attack of water at the formal Ru<sup>V</sup>=O, oxygen of the closely placed pendant carboxylic group reacts with Ru<sup>V</sup>=O to form the ruthenium-

(III) percarboxylate intermediate that is attacked by water in the follow-up steps. The labeling experiment with <sup>18</sup>O-labeled water confirms the incorporation of a labeled oxygen isotope into the carboxylic group of **2**<sup>Aq</sup> under catalytic conditions. Here we provide for the first time experimental evidence of the oxide relay functionality of the pendant carboxylic group for a remarkable rate enhancement toward water oxidation, supporting the prediction by Ahlquist et al. computationally.<sup>20</sup> Thus, the present study might help to develop the next generation of advanced catalysts by judiciously incorporating a carboxylic group into the ligand scaffold.

## ASSOCIATED CONTENT

### Supporting Information

The Supporting Information is available free of charge at <https://pubs.acs.org/doi/10.1021/acs.inorgchem.1c03105>.

Experimental section, physical measurements, computational methods, additional compound characterization data, experimental results, spin-density plots, and coordinates of the optimized structures (PDF)

## Accession Codes

CCDC 2107197 contains the supplementary crystallographic data for this paper. These data can be obtained free of charge via [www.ccdc.cam.ac.uk/data\\_request/cif](http://www.ccdc.cam.ac.uk/data_request/cif), or by emailing [data\\_request@ccdc.cam.ac.uk](mailto:data_request@ccdc.cam.ac.uk), or by contacting The Cambridge Crystallographic Data Centre, 12 Union Road, Cambridge CB2 1EZ, UK; fax: +44 1223 336033.

## AUTHOR INFORMATION

### Corresponding Author

**Sukanta Mandal** – Department of Chemistry, Indian Institute of Technology (IIT) Kharagpur, Kharagpur 721302, India;  
orcid.org/0000-0001-6456-3898;  
Email: [sukanta.mandal@chem.iitkgp.ac.in](mailto:sukanta.mandal@chem.iitkgp.ac.in)

### Authors

**Animesh Kundu** – Department of Chemistry, Indian Institute of Technology (IIT) Kharagpur, Kharagpur 721302, India  
**Suman K. Barman** – Department of Chemical Sciences, Indian Institute of Science Education and Research (IISER) Mohali, Manauli 140306, India

Complete contact information is available at:  
<https://pubs.acs.org/10.1021/acs.inorgchem.1c03105>

### Author Contributions

The manuscript was prepared through contributions of all authors. All authors have given approval to the final version of the manuscript. A.K. synthesized all of the complexes and performed all experimental works. S.K.B. performed DFT calculations. S.M. conceived the project, analyzed the data, and wrote the paper.

### Notes

The authors declare no competing financial interest.

## ACKNOWLEDGMENTS

The project is funded by the Council of Scientific and Industrial Research, Government of India [Grant 01(3052)/21/EMR-II to S.M.]. S.M. thanks to SERB, New Delhi, India, for a research grant (Grant EMR/2015/001136) to procure the electrochemical analyzer. A.K. thanks IIT Kharagpur for a Ph.D. fellowship. We are thankful to the Department of Science and Technology (DST), Government of India, under the DST-FIST programme for the NMR (SR/FST/CSII-026/2013) facilities to the Department of Chemistry, IIT Kharagpur. We thank the Central Research Facility, IIT Kharagpur, for providing access to the Raman instrument. We also thank the Department of Chemistry, IIT Kharagpur, for providing infrastructural and other major instrumental facilities (X-ray, FTIR-ATR, CHN, HRMS, etc.). S.K.B. gratefully acknowledges a startup grant from IISER Mohali. We thank the reviewers for valuable notes at the revision stage.

## REFERENCES

- (1) Concepcion, J. J.; House, R. L.; Papanikolas, J. M.; Meyer, T. J. Chemical Approaches to Artificial Photosynthesis. *Proc. Natl. Acad. Sci. U. S. A.* **2012**, *109*, 15560–15564.
- (2) El-Khouly, M. E.; El-Mohsawy, E.; Fukuzumi, S. Solar Energy Conversion: From Natural to Artificial Photosynthesis. *J. Photochem. Photobiol. C: Photochem. Rev.* **2017**, *31*, 36–83.
- (3) Gust, D.; Moore, T. A.; Moore, A. L. Solar Fuels via Artificial Photosynthesis. *Acc. Chem. Res.* **2009**, *42*, 1890–1898.
- (4) Berardi, S.; Drouet, S.; Francas, L.; Gimbert-Surinach, C.; Guttentag, M.; Richmond, C.; Stoll, T.; Llobet, A. Molecular Artificial Photosynthesis. *Chem. Soc. Rev.* **2014**, *43*, 7501–7519.
- (5) (a) Sala, X.; Maji, S.; Bofill, R.; Garcia-Anton, J.; Escriche, L.; Llobet, A. Molecular Water Oxidation Mechanisms Followed by Transition Metals: State of the Art. *Acc. Chem. Res.* **2014**, *47*, 504–516. (b) Shaffer, D. W.; Xie, Y.; Concepcion, J. J. O–O Bond Formation in Ruthenium-Catalyzed Water Oxidation: Single-Site Nucleophilic Attack vs. O–O Radical Coupling. *Chem. Soc. Rev.* **2017**, *46*, 6170–6193.
- (6) Karkas, M. D.; Verho, O.; Johnston, E. V.; Akermark, B. Artificial Photosynthesis: Molecular Systems for Catalytic Water Oxidation. *Chem. Rev.* **2014**, *114*, 11863–12001.
- (7) Matheu, R.; Garrido-Barros, P.; Gil-Sepulcre, M.; Ertem, M. Z.; Sala, X.; Gimbert-Surinach, C.; Llobet, A. The Development of Molecular Water Oxidation Catalysts. *Nat. Rev. Chem.* **2019**, *3*, 331–341.
- (8) Sutradhar, M.; Pombeiro, A. J. L.; da Silva, J. A. L. Water Oxidation with Transition Metal Catalysts with Non-Innocent Ligands and its Mechanisms. *Coord. Chem. Rev.* **2021**, *439*, 213911–213929.
- (9) Matias, T. A.; Keppler, A. F.; Bartoloni, F. H. In Need of a Second-Hand? The Second Coordination Sphere of Ruthenium Complexes Enables Water Oxidation with Improved Catalytic Activity. *Dalton Trans.* **2020**, *49*, 16034–16046.
- (10) (a) Yoshida, M.; Kondo, M.; Torii, S.; Sakai, K.; Masaoka, S. Oxygen Evolution Catalyzed by a Mononuclear Ruthenium Complex Bearing Pendant SO<sub>3</sub><sup>−</sup> Groups. *Angew. Chem., Int. Ed.* **2015**, *54*, 7981–7984. (b) Yi, J.; Zhan, S.; Chen, L.; Tian, Q.; Wang, N.; Li, J.; Xu, W.; Zhang, B.; Ahlquist, M. S. G. Electrostatic Interactions Accelerating Water Oxidation Catalysis via Intercatalyst O–O Coupling. *J. Am. Chem. Soc.* **2021**, *143*, 2484–2490.
- (11) Das, B.; Rahaman, A.; Shatskiy, A.; Verho, O.; Karkas, M. D.; Akermark, B. The Impact of Ligand Carboxylates on Electrocatalyzed Water Oxidation. *Acc. Chem. Res.* **2021**, *54*, 3326–3337.
- (12) Duan, L.; Bozoglian, F.; Mandal, S.; Stewart, B.; Privalov, T.; Llobet, A.; Sun, L. A Molecular Ruthenium Catalyst with Water-Oxidation Activity Comparable to that of Photosystem II. *Nat. Chem.* **2012**, *4*, 418–423.
- (13) Matheu, R.; Ertem, M. Z.; Benet-Buchholz, J.; Coronado, E.; Batista, V. S.; Sala, X.; Llobet, A. Intramolecular Proton Transfer Boosts Water Oxidation Catalyzed by a Ru Complex. *J. Am. Chem. Soc.* **2015**, *137*, 10786–10795.
- (14) Vereshchuk, N.; Matheu, R.; Benet-Buchholz, J.; Pipelier, M.; Lebreton, J.; Dubreuil, D.; Tessier, A.; Gimbert-Surinach, C.; Ertem, M. Z.; Llobet, A. Second Coordination Sphere Effects in an Evolved Ru Complex Based on Highly Adaptable Ligand Results in Rapid Water Oxidation Catalysis. *J. Am. Chem. Soc.* **2020**, *142*, 5068–5077.
- (15) Nash, A. G.; Breyer, C. J.; Vincenzini, B. D.; Elliott, G. I.; Niklas, J.; Poluektov, O. G.; Rheingold, A. L.; Smith, D. K.; Musaev, D. G.; Grotjahn, D. B. An Active-Site Sulfonate Group Creates a Fast Water Oxidation Electrocatalyst That Exhibits High Activity in Acid. *Angew. Chem., Int. Ed.* **2021**, *60*, 1540–1545.
- (16) Kagalwala, H. N.; Tong, L.; Zong, R.; Kohler, L.; Ahlquist, M. S. G.; Fan, T.; Gagnon, K. J.; Thummel, R. P. Evidence for Oxidative Decay of a Ru-Bound Ligand during Catalyzed Water Oxidation. *ACS Catal.* **2017**, *7*, 2607–2615.
- (17) Hoque, Md A.; Chowdhury, A. D.; Maji, S.; Benet-Buchholz, J.; Ertem, M. Z.; Gimbert-Surinach, C.; Lahiri, G. K.; Llobet, A. Synthesis, Characterization, and Water Oxidation Activity of Isomeric Ru Complexes. *Inorg. Chem.* **2021**, *60*, 5791–5803.
- (18) (a) Kundu, A.; Dey, S. K.; Dey, S.; Anoop, A.; Mandal, S. Mononuclear Ruthenium-Based Water Oxidation Catalyst Supported by Anionic, Redox-Non-Innocent Ligand: Heterometallic O–O Bond Formation via Radical Coupling Pathway. *Inorg. Chem.* **2020**, *59*, 1461–1470. (b) Karkas, M. D.; Li, Y.-Y.; Siegbahn, P. E. M.; Liao, R.-Z.; Akermark, B. Metal–Ligand Cooperation in Single-Site Ruthenium Water Oxidation Catalysts: A Combined Experimental and Quantum Chemical Approach. *Inorg. Chem.* **2018**, *57*, 10881–

10895. (c) Hoque, Md A.; Benet-Buchholz, J.; Llobet, A.; Gimbert-Surinach, C. Catalytic Oxidation of Water to Dioxygen by Mononuclear Ru Complexes Bearing a 2,6-Pyridinedicarboxylate Ligand. *ChemSusChem* **2019**, *12*, 1949–1957. (d) Lu, Z.; Gao, Y.; Chen, H.; Liu, Z.; Chen, L.; Sun, L. Efficient Molecular Ruthenium Catalysts Containing Anionic Ligands for Water Oxidation. *Dalton Trans.* **2016**, *45*, 18459–18464. (e) Abdel-Magied, A. F.; Shatskiy, A.; Liao, R.-Z.; Laine, T. M.; Arafa, W. A. A.; Siegbahn, P. E. M.; Karkas, M. D.; Akermark, B.; Johnston, E. V. Chemical and Photochemical Water Oxidation Mediated by an Efficient Single-Site Ruthenium Catalyst. *ChemSusChem* **2016**, *9*, 3448–3456. (f) Sander, A. C.; Maji, S.; Francas, L.; Bohnisch, T.; Dechert, S.; Llobet, A.; Meyer, F. Highly Efficient Binuclear Ruthenium Catalyst for Water Oxidation. *ChemSusChem* **2015**, *8*, 1697–1702.

(19) (a) Umena, Y.; Kawakami, K.; Shen, J. R.; Kamiya, N. Crystal Structure of Oxygen-Evolving Photosystem II at a Resolution of 1.9 Å. *Nature* **2011**, *473*, 55–60. (b) Nakamura, S.; Noguchi, T. Quantum Mechanics/Molecular Mechanics Simulation of the Ligand Vibrations of the Water-Oxidizing Mn<sub>4</sub>CaO<sub>5</sub> Cluster in Photosystem II. *Proc. Natl. Acad. Sci. U. S. A.* **2016**, *113*, 12727–12732.

(20) Zhan, S.; De Gracia Trivino, J. A.; Ahlquist, M. S. G. The Carboxylate Ligand as an Oxide Relay in Catalytic Water Oxidation. *J. Am. Chem. Soc.* **2019**, *141*, 10247–10252.

(21) Chanda, N.; Paul, D.; Kar, S.; Mobin, S. M.; Datta, A.; Puranik, V. G.; Rao, K. K.; Lahiri, G. K. Effect of 2-(2-Pyridyl)azole-Based Ancillary Ligands (L<sup>1-4</sup>) on the Electrophilicity of the Nitrosyl Function in [Ru<sup>II</sup>(trpy)(L<sup>1-4</sup>)(NO)]<sup>3+</sup> [trpy = 2,2':6',2''-Terpyridine]. Synthesis, Structures, and Spectroscopic, Electrochemical, and Kinetic Aspects. *Inorg. Chem.* **2005**, *44*, 3499–3511.

(22) Xue, F.; Luo, X.; Ye, C.; Ye, W.; Wang, Y. Inhibitory Properties of 2-Substituent-1H-Benzimidazole-4-Carboxamide Derivatives Against Enteroviruses. *Bioorg. Med. Chem.* **2011**, *19*, 2641–2649.

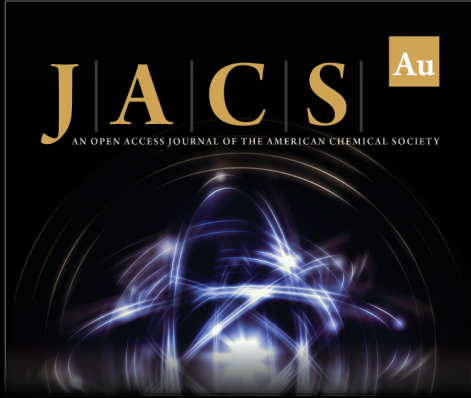
(23) Kundu, A.; Khan, S.; Dey, S.; Dutta, C.; Anoop, A.; Mandal, S. Synthesis and Physicochemical Properties of Ruthenium(II) Complexes Having Pentadentate Scaffolds: Water Oxidation Activity and Deactivation Pathway. *Eur. J. Inorg. Chem.* **2019**, *2019*, 164–177.

(24) Takeuchi, K. J.; Thompson, M. S.; Pipes, D. W.; Meyer, T. J. Redox and Spectral Properties of Monooxo Polypyridyl Complexes of Ruthenium and Osmium in Aqueous Media. *Inorg. Chem.* **1984**, *23*, 1845–1851.

(25) (a) Karkas, M. D.; Liao, R.-Z.; Laine, T. M.; Akermark, T.; Ghanem, S.; Siegbahn, P. E. M.; Akermark, B. Molecular Ruthenium Water Oxidation Catalysts Carrying Non-Innocent Ligands: Mechanistic Insight Through Structure–Activity Relationships and Quantum Chemical Calculations. *Catal. Sci. Technol.* **2016**, *6*, 1306–1319. (b) Marenich, A. V.; Majumdar, A.; Lenz, M.; Cramer, C. J.; Truhlar, D. G. Construction of Pourbaix Diagrams for Ruthenium-Based WaterOxidation Catalysts by Density Functional Theory. *Angew. Chem., Int. Ed.* **2012**, *51*, 12810–12814. (c) Marenich, A. V.; Ho, J.; Coote, M. L.; Cramer, C. J.; Truhlar, D. G. *Phys. Chem. Chem. Phys.* **2014**, *16*, 15068–15106.


(26) Chen, Z.; Concepcion, J. J.; Meyer, T. J. Rapid Catalytic Water Oxidation by a Single Site, Ru Carbene Catalyst. *Dalton Trans.* **2011**, *40*, 3789–3792.


(27) Ye, S.; Neese, F. Nonheme Oxo-Iron(IV) Intermediates form an Oxyl Radical upon Approaching the C–H Bond Activation Transition State. *Proc. Natl. Acad. Sci. U. S. A.* **2011**, *108*, 1228–1233.



**JACS** Au  
AN OPEN ACCESS JOURNAL OF THE AMERICAN CHEMICAL SOCIETY

Editor-in-Chief  
**Prof. Christopher W. Jones**  
Georgia Institute of Technology, USA

**Open for Submissions** 

pubs.acs.org/jacsau  ACS Publications  
Most Trusted. Most Cited. Most Read.